J. Fluid Mech. (1992), *vol.* 236, *pp.* 43–59
Printed in Great Britain

Complete adiabatic evaporation of highly superheated liquid jets

By TH. KURSCHAT, H. CHAVES AND G. E. A. MEIER
Max-Planck-Institut for Strömungsforschung, D-3400 Göttingen, Germany

(Received 6 August 1990 and in revised form 13 May 1991)

A nozzle expansion into a vacuum chamber was used to investigate the evaporation of highly superheated liquid jets. The large molar specific heat of fluids with high molecular complexity – in this case C_6F_{14} – is responsible for the new phenomena reported here. A model was developed to describe the basic physical effects. A cubic equation of state was used to describe the thermodynamic properties of the fluid. The evaporation was modelled as a sonic deflagration followed by an axisymmetric supersonic expansion. As in the case of hypersonic gas jets the final state is reached by a normal shock. For sufficiently high temperatures and expansion ratios a complete adiabatic evaporation of the liquid was found. At even higher temperatures the liquid evaporates completely within a rarefaction discontinuity. The predictions of the model are in good agreement with the experimental results.

1. Introduction and background

Substances of high molecular complexity, i.e. substances of large molar specific heat, are very common in everyday life – for example hydrocarbons, commonly used as liquid fuels. It is known, both from theoretical (Thompson & Sullivan 1975) and experimental (Dettleff *et al.* 1979) studies, that these substances can undergo complete phase transitions by a purely adiabatic process. This can be seen clearly from the behaviour of the phase boundary in temperature–entropy diagrams (figure 1), where isentropic processes are represented by vertical arrows. For small temperature differences between initial and end state, the difference between adiabatic processes with dissipation and isentropic processes is a slight increase in entropy. Figure 1 (*a*) shows the phase boundary for a substance with high molecular complexity ($c_v^* = 39.3$). In figure 1 (*b*) the phase boundary for water as an example of a substance with low molar specific heat ($c_v^* = 3.4$) is plotted for comparison. The parameter $c_v^* = c_v^0(T = T_c)/R$ denotes the molar ideal-gas specific heat at constant volume at the critical temperature (point C) normalized by the gas constant R, i.e. c_v^0 is the specific heat at constant volume which depends only on temperature. Because for ideal gases the specific heat is only dependent on temperature, this part of the specific heat for a real gas is called its ideal-gas specific heat, denoted by the superscript 0. It can be shown (Thompson, Carofano & Kim 1986) that c_v^* is the crucial parameter for the tendency of the saturated vapour boundary to lean to the right in the temperature–entropy plane. With increasing specific heat the slope of the phase boundary on the vapour side changes sign and becomes positive (retrograde). This leads to the so-called retrograde behaviour of substances with large molar specific heat, for example liquefaction shocks and complete adiabatic phase transitions.

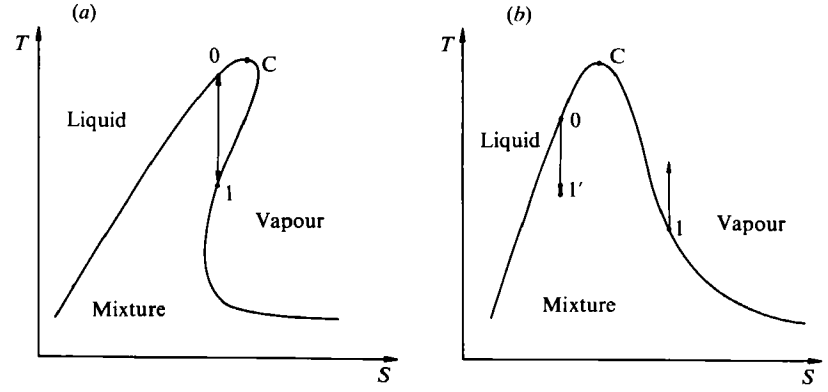

FIGURE 1. Temperature–entropy diagrams for substances with large and small molar heat: (a) $c_v^* = 39.3$, (b) $c_v^* = 3.4$.

Physically, the difference between substances of small and large molar specific heat is due to the large number of internal molecular degrees of freedom of the latter. This characterizes the ability of the molecule to store internal energy. Therefore each molecular of a substance of large molar specific heat can store and give up large amounts of energy which can exceed the latent heat of evaporation. In this case phase transitions are possible on a molecular scale and are not limited by heat conduction. Since the latent heat of evaporation does not depend strongly on molecular complexity, but is basically a decreasing function of temperature while the internal energy increases with temperature, this effect is most pronounced with increasing temperature.

Surprising wave phenomena like rarefaction shocks (Sidorenko 1968, 1982; Borisov *et al.* 1983; Lambrakis & Thompson 1972; Thompson & Lambrakis 1973), liquefaction shock waves, evaporation waves and wave splitting (Chaves *et al.* 1985; Dettleff *et al.* 1982; Thompson *et al.* 1987) enrich the gasdynamics of retrograde fluids. In particular, complete adiabatic phase transitions, which are only possible for retrograde substances, have been investigated intensively in the past. Complete adiabatic liquefaction was achieved first in shock tube experiments, but complete adiabatic evaporation could not be obtained by blowdown experiments in a one-dimensional duct (Chaves 1984). This was due to a sonic state in the duct limiting the expansion ratio of these experiments.

The aim of the present work is to verify the complete adiabatic evaporation by a jet expansion and to develop a model describing the basic physical effects occurring in the jet flow. Some of the results were previously presented at the IUTAM Symposium by Chaves, Kurschat & Meier (1990) and are now described in detail.

2. Experimental set-up

Figure 2 shows a global scheme of the experimental set-up. Most of the equipment is needed to set-up the initial conditions for the experiments, i.e. initial temperature T_0 and pressure p_0 of the liquid and final pressure p_e in the 1 m^3 expansion chamber. These are the variable parameters in the experiments. The initial temperature could be varied between room temperature and 180 °C, the initial pressure between atmospheric and 20 bar, and the final pressure between atmospheric and 10^{-2} mbar. By measuring the displacement of the bellows and the opening time of the nozzle, the volumetric flow rate could be measured within an accuracy of 3%. The bellows also

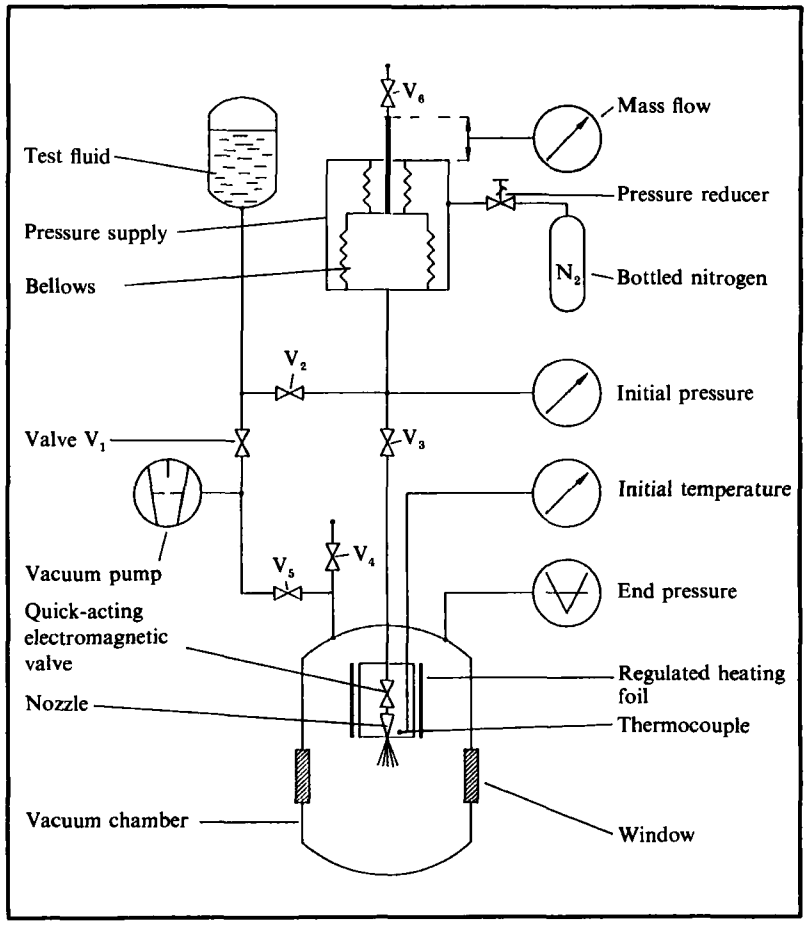

FIGURE 2. Experimental set-up.

inhibited contact of the pressurizing nitrogen with the liquid, thus preventing gas dissolving in the liquid.

The density field of the jet flow could be visualized using a differential interferometer, as shown in figure 3. By removing the Wollaston prisms and the polarization filters, shadowgraphs could be made, which show the opaque liquid part of the jet only. The images were recorded by a video camera and printed by a video printer. Both techniques, interferometry and shadowgraphs, used together yield a clear picture of the two-phase flow. A fast LED-flash was used for illumination. Typical exposure times were about 5 μs.

A continuous experiment would require a pump of high capacity to keep the final pressure constant, since the rate of vapour production by the evaporating jet is large. Therefore short-time experiments were carried out during the opening time of an electrically driven injector valve (typically 10–40 ms). The flow becomes stationary after a period of approximately 1 ms. This was checked by experiments with different delay times of the LED-flash after the opening of the injector valve. Because of the large volume of the expansion chamber, even twenty single injections did not change the final pressure significantly.

A convergent nozzle of 0.35 mm exit diameter, a length-to-exit-diameter ratio of 5.7 and a convergence half-angle of 10° was used. This particular nozzle geometry

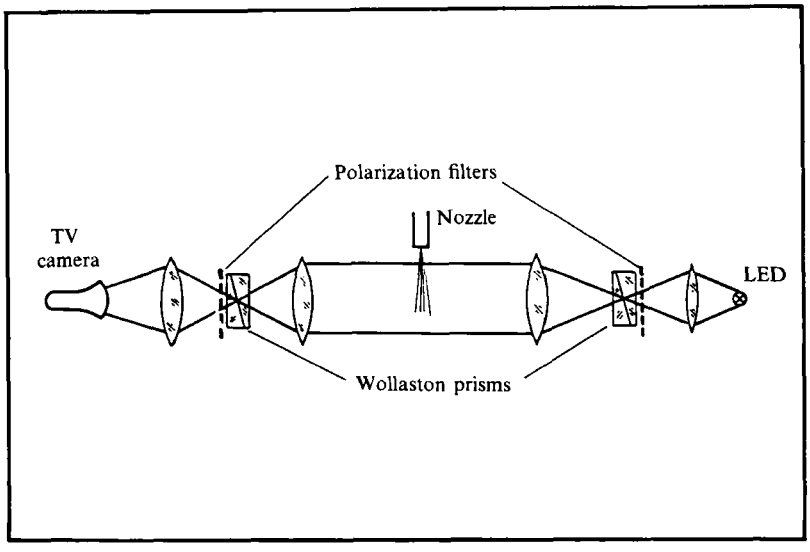

FIGURE 3. Optical set-up of the differential interferometer.

ensures a quick and unperturbed expansion of the liquid from a subcooled to a superheated state. C_6F_{14} was used as test substance in this work for practical reasons. The critical values are $T_c = 178$ °C, $p_c = 18.7$ bar, $V_c = 1.58$ l/kg, and $c_v^* = 39.3$.

3. Initial observations on the results

Different types of jets can be observed depending on the initial temperature T_0 and final pressure p_e, i.e. depending on the superheat $H = p_s(T_0)/p_e$. The pressure $p_s(T_0)$ denotes the vapour pressure with respect to the initial temperature. The results obtained range from mechanically and thermodynamically stable subcooled liquid jets ($H < 1$; figure 4*a*) through superheated liquid jets to underexpanded supersonic gas jets (figure 4*f*), where the initial state is gaseous and the flow is mainly determined by the expansion ratio p_0/p_e.

If the final pressure is higher than the vapour pressure of the liquid ($H < 1$), the jet remains in a liquid state and is thermodynamically stable. Because of the low compressibility of the liquid, the temperature decrease due to the expansion of the liquid within the nozzle is small. Therefore the temperature of the liquid at the nozzle exit is close to the initial temperature, as long as the fluid issuing from the nozzle is pure liquid. With increasing initial temperature or decreasing final pressure the vapour pressure of the liquid jet can exceed the final pressure ($H > 1$). Then the jet is superheated. With increasing superheat the jet first breaks up at singular points where heterogeneous nucleation nuclei grow to form large bubbles (figure 4*b*). At somewhat larger superheat levels, the number of nuclei increases and the growth of the bubbles produces pressure disturbances which trigger further nucleation events (see Lienhard & Day 1970; Fuchs & Legge 1979), or the jet breaks up after remaining intact up to a length (figure 4*c*) given by the mean lifetime of the superheated liquid state (see Skripov 1974) and the exit velocity. These jets are usually referred to as flashing jets and investigations of them have been reported in the literature cited above. In these cases the whole jet flow remains subsonic.

With decreasing final pressure and/or increasing initial temperature, however, the evaporation rate at the jet surface increases and becomes so high that sonic

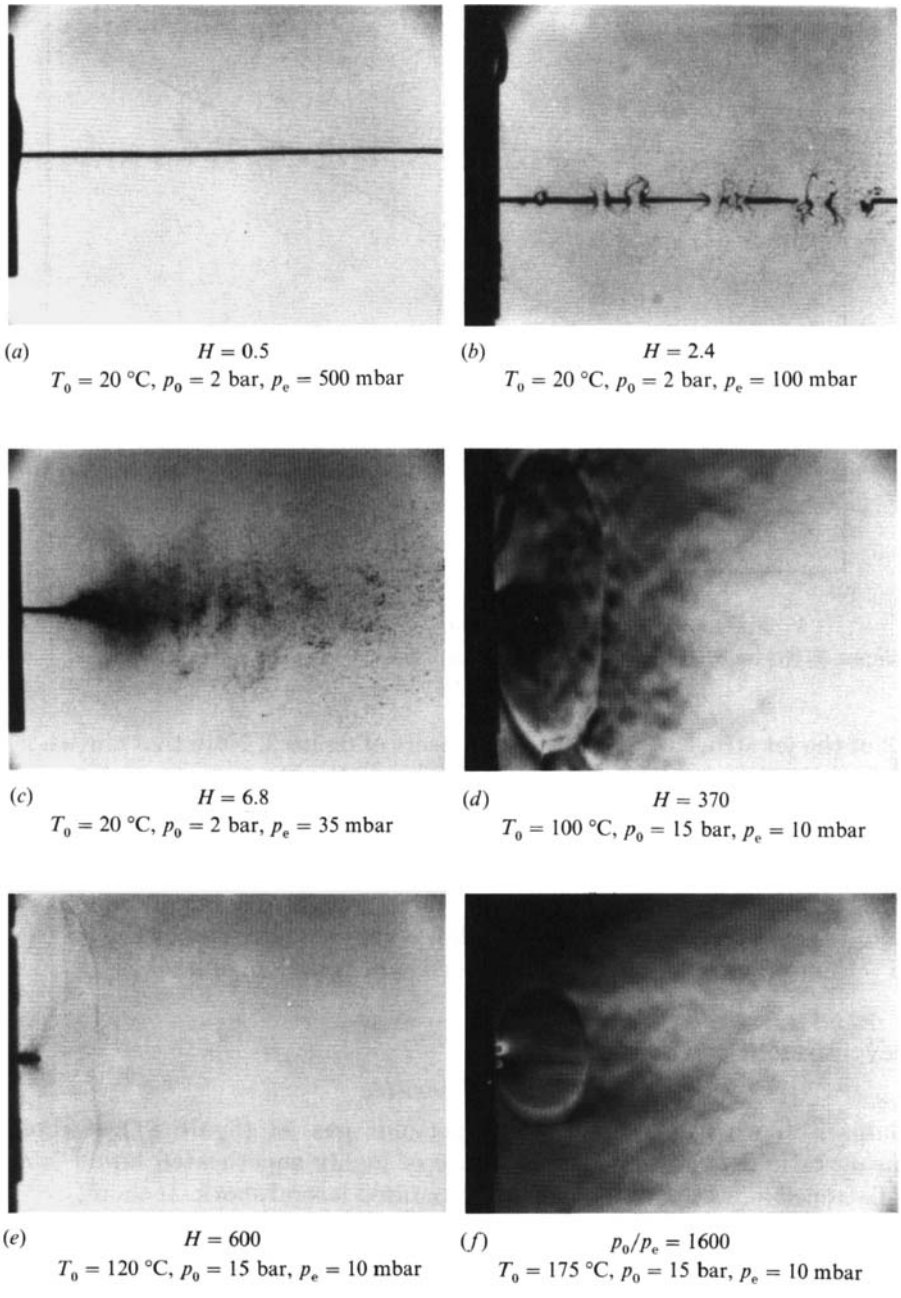

(*a*) $H = 0.5$
$T_0 = 20$ °C, $p_0 = 2$ bar, $p_e = 500$ mbar

(*b*) $H = 2.4$
$T_0 = 20$ °C, $p_0 = 2$ bar, $p_e = 100$ mbar

(*c*) $H = 6.8$
$T_0 = 20$ °C, $p_0 = 2$ bar, $p_e = 35$ mbar

(*d*) $H = 370$
$T_0 = 100$ °C, $p_0 = 15$ bar, $p_e = 10$ mbar

(*e*) $H = 600$
$T_0 = 120$ °C, $p_0 = 15$ bar, $p_e = 10$ mbar

(*f*) $p_0/p_e = 1600$
$T_0 = 175$ °C, $p_0 = 15$ bar, $p_e = 10$ mbar

FIGURE 4. Jets of different types, depending on the superheat H of the liquid. $H = p_s(T_0)/p_e$ is the ratio of the vapour pressure corresponding to the initial temperature to the final pressure. H is only a qualitative measure of the superheat of the liquid, because the pressure within the supersonic region is different from the final pressure.

conditions are reached and the jet structure changes radically (figure 4*d*). These are the jets this paper deals with. The jet structure is composed of a liquid core surrounded by a supersonic two-phase-flow region terminated by a barrel shock, a quasi-cylindrical lateral shock, and a Mach-disc. At the intersection between two of these shocks, triple points (also called Mach reflections) are present. A schematic

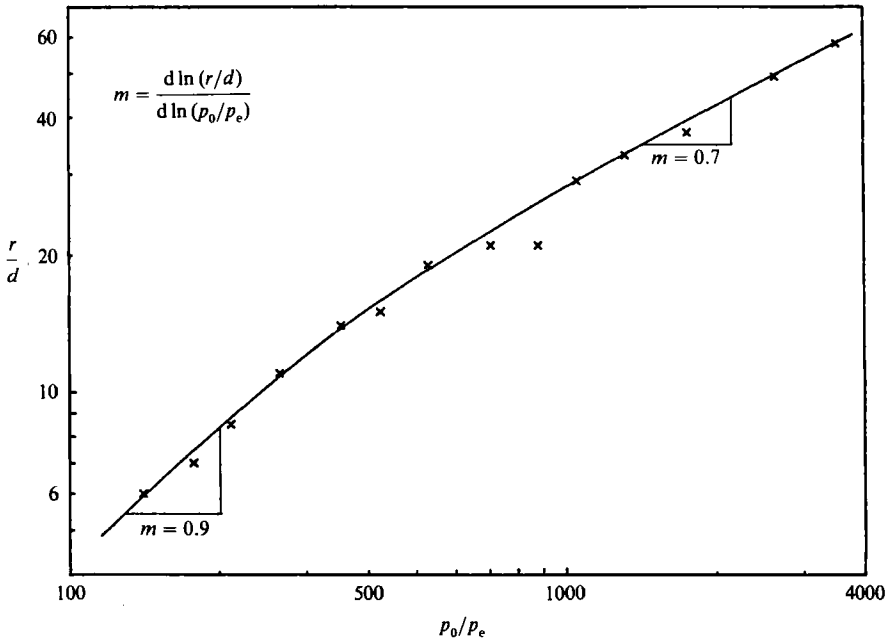

FIGURE 5. Normalized distance of the lateral shock versus the pressure ratio. $T_0 = 57$ °C, $p_0 = 10.6$ bar.

sketch of the jet structure is given in the insert of figure 9. Note that the whole shock structure is stationary. Both the barrel shock and the Mach-disc are phenomena well known from studies of underexpanded supersonic gas jets (see for example figure 4*f*). The cylindrical shock however is new, and gives the decisive clue to the phenomena occurring in the jet. As the superheat increases, the droplet cloud around the liquid jet core becomes smaller. At least at very high superheat levels, it can be seen that the liquid is evaporating completely within a very small region at the surface of the liquid jet core (figure 4*e*), and the droplet cloud is no longer visible.

4. Development of the model

4.1. *Geometry*

In comparison with underexpanded supersonic gas jet (figure 4*f*) of comparable expansion ratio p_0/p_e, the shock structure of highly superheated liquid jets (figure 4*d*) is flattened like a pancake and has a separated lateral shock. It therefore becomes clear that the flow is dominated by a cylindrical flow symmetry, and a supersonic source flow with a cylindrical terminating shock is proposed. This is an analogy to the spherical source flow model with a terminating Mach-disc, which is often used for underexpanded supersonic gas jets (Ashkenas & Sherman 1967). According to this model it can be shown that the normalized distance of the Mach-disc from the nozzle exit r/d – where d is the nozzle diameter – is a function mainly of the square root of the pressure ratio p_0/p_e alone (Kurschat, Chaves & Meier 1991). Because of the similarity of supersonic flows, the distance of a cylindrical shock from the jet axis, produced by a line source, should be a nearly linear function of the pressure ratio only.

In figure 5 the measured normalized (with the nozzle diameter) distance of the lateral cylindrical shock is plotted versus the pressure ratio. On a double logarithmic

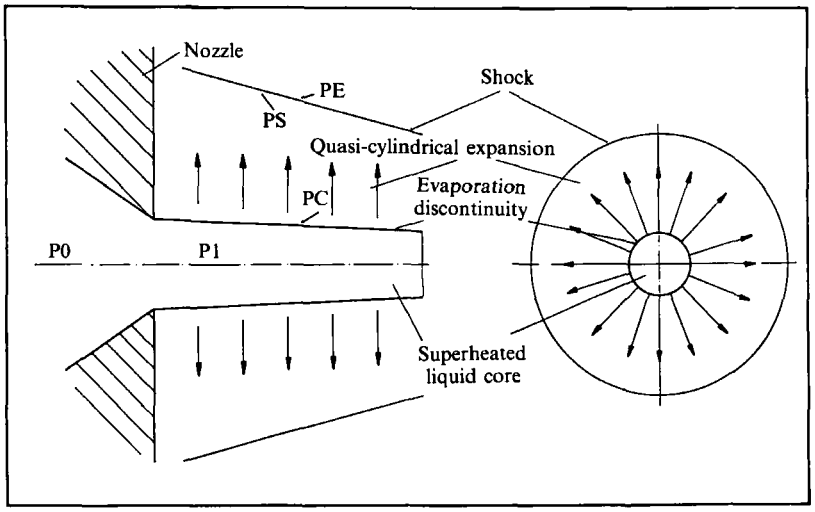

FIGURE 6. Geometry of the evaporating jet.

plot, a slope of this curve equal to unity corresponds to axisymmetric source flow. A slope of 0.5 would indicate the presence of a spherical flow geometry. Figure 5 shows that for small shock distances a linear approximation is nearly valid. Because of the finite length of the liquid jet core, which is the physical line source in this case, the deviation from linearity becomes greater for large r/d, but the assumption of an axisymmetric expansion seems to be reasonable.

Another strong hint towards an adequate jet model is given by figure 4(*e*), as it gives the answer to the important question of transition from subsonic to supersonic flow. Here again the differences from supersonic gas jets are very instructive. Sonic flow conditions in underexpanded supersonic gas jets are reached by isentropic expansion at the narrowest cross-section of the nozzle. This leads to choking of the mass flow rate and a spherical flow near the jet axis. But for initial temperatures $T_0 < 130$ °C measurements of the mass flow rate (figure 11) show no choking for superheated liquid jets, although a supersonic flow region and an extremely flattened shock structure are present. This indicates clearly that the velocity at the nozzle exit must be subsonic. The absence of a minimum cross-section downstream of the nozzle exit leads to the conclusion that the sonic state cannot be reached by an isentropic process, but must be attained by means of a non-isentropic (expansion) discontinuity. This discontinuity is seen on figure 4(*e*) at the surface of the liquid jet core, where the evaporation takes place within a very thin region. The dimensions of this region are small in comparison with the lengthscales of the global flow. Therefore the evaporation region can be regarded as a discontinuity in the flow field. The geometry of this region is a truncated quasi-cylindrical cone. In §4.2 it will be shown that the downstream state of this evaporation discontinuity has sonic conditions, that the liquid of the jet core must be strongly superheated and that the discontinuity can be uniquely determined.

In figure 6 the hypothesized geometry of the flow model is sketched. The model is basically one-dimensional. The states denoted by P0, P1, PC, PS and PE are described at the beginning of §4.3 where the thermodynamical model is presented.

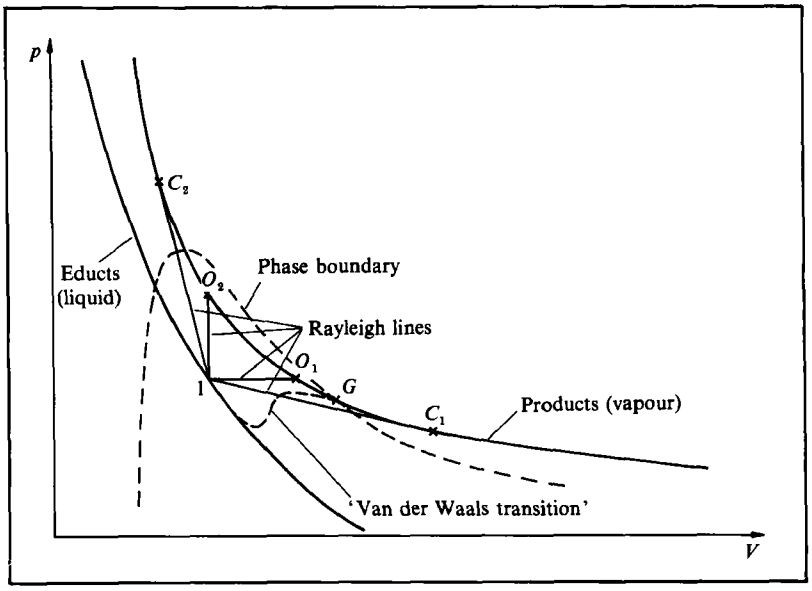

FIGURE 7. Detonation adiabat and relationship to the evaporation discontinuity.

4.2. *Modelling the evaporation*

Most important for the model presented here is an adequate formulation of the evaporation process and the mechanism which leads to supersonic flow. The observations presented in the preceding section lead to the conclusion that the transition to supersonic flow and the evaporation take place within an expansion discontinuity.

Such changes of state are common in the theory of flow discontinuities with chemical reactions (i.e. combustion, detonation), and especially of flame propagation; they are called deflagrations. Figure 7 shows the detonation adiabat (see for example Landau & Lifshitz 1966), which is described by the Rankine–Hugoniot equation:

$$h_1(V_1, p_1) - h_2(V_2, p_2) = \tfrac{1}{2}(V_1 + V_2)(p_1 - p_2). \tag{1}$$

V, p, h denote the specific volume, the pressure and the specific enthalpy, respectively.

The upper line in figure 7 satisfies the Rankine–Hugoniot equation with respect to the state upstream of the discontinuity denoted by 1. This state also lies on a curve which satisfies the Rankine–Hugoniot equation but without the (usually chemical) reaction of the substances upstream (educts). Then the functions $h_1(V, p)$ and $h_2(V, p)$ are identical. But here h_1 and h_2 are not the same functions because of the chemical reaction (phase transition). The broken lines indicate the analogy to the evaporation of a superheated liquid, if liquid and gaseous phases of the substance can be described by a common thermal equation of state, as for example by a van der Waals equation. Then state 1 can be regarded as superheated liquid and the states to the right of O_1 as gaseous or mixed states, and the evaporation itself can be described as a deflagration. The slopes of the Rayleigh lines and the Rankine–Hugoniot adiabats at their points of intersection indicate that deflagrations with downstream state between O_1 and C_1 have subsonic outflow and those with downstream states to the right of C_1 have supersonic outflow. In both cases the upstream states are subsonic. At point C_1, sonic conditions and a maximum mass flow (= evaporation rate) across the discontinuity are reached.

Following Landau & Lifshitz (1966), a stability analysis for discontinuities shows that the mass flow rate for a deflagration with subsonic inflow velocity and subsonic outflow velocity has to be determined by a rate of reaction. In the case of a combustion flame this rate is normally determined by diffusion or thermal conductivity. In the case presented here the reaction rate is replaced by the evaporation rate, which in turn is a gas kinetic process at the liquid surface. For substances with retrograde behaviour the evaporation takes place on a molecular scale and is not limited by heat conduction as for normal substances. So the evaporation rate is limited by the nucleation rate and therefore by the superheat of the liquid jet core. Point C_1 on figure 7 is a Chapman–Jouguet point and yields the maximum evaporation rate for a given state 1 and sonic outflow conditions. A supersonic outflow (states to the right of C_1) is not possible because a further condition is necessary for stability which is not available in this case. This means that supersonic deflagrations are not possible without a further boundary condition from outside. The experimental results however demand at least sonic outflow conditions. So as a result we find that the experimentally observed phenomena can be described only by a sonic deflagration.

The quantitative calculations presented in the next section show that the velocity of the evaporation discontinuity is smaller than the velocity of the nozzle flow by a factor of 200. Therefore stationary flow is only possible when the deflagration travels almost perpendicularly to the nozzle flow, i.e. forms the surface of the liquid jet core of axisymmetric geometry.

The construction of the sonic deflagration (tangent at the detonation adiabat) and the superheated state 1 in figure 7 (P1 in figure 8) is unique because an increasing superheat will result in an increase of the nucleation and evaporation rates. On the other hand an increased superheat means a lower pressure at state 1 and therefore a smaller slope of the Rayleigh line, given by

$$-j^2 = \frac{p_2 - p_1}{V_2 - V_1}. \tag{2}$$

This means a smaller mass flow rate j across the discontinuity which limits the evaporation rate necessary for stability. The process is therefore self-adjusting and stable.

If complete evaporation cannot be reached within the evaporation discontinuity, then the downstream state is a two-phase sonic state and the phase transition goes on in a further isentropic two-phase supersonic expansion.

4.3. *Closing the model*

Figure 8 schematically shows the thermodynamical model in a reduced pressure–volume plane. The liquid is isentropically expanded within the nozzle from the initial state P0 to a superheated state P1 at the exit of the nozzle. The evaporation occurs within a discontinuity described as a deflagration from state P1 to state PC. Sonic conditions are reached at PC on the surface of the superheated liquid jet. PC is the initial state for the following axisymmetric supersonic expansion to state PS upstream of the lateral closing shock. This shock to the final state PE has to match the experimentally given final pressure p_e.

In order to plot the whole sequence of changes of state on one diagram, the abscissa in figure 8 has been plotted logarithmically and the ordinate has been distorted in a nonlinear manner. As a consequence the curvature of the equilibrium Rankine–

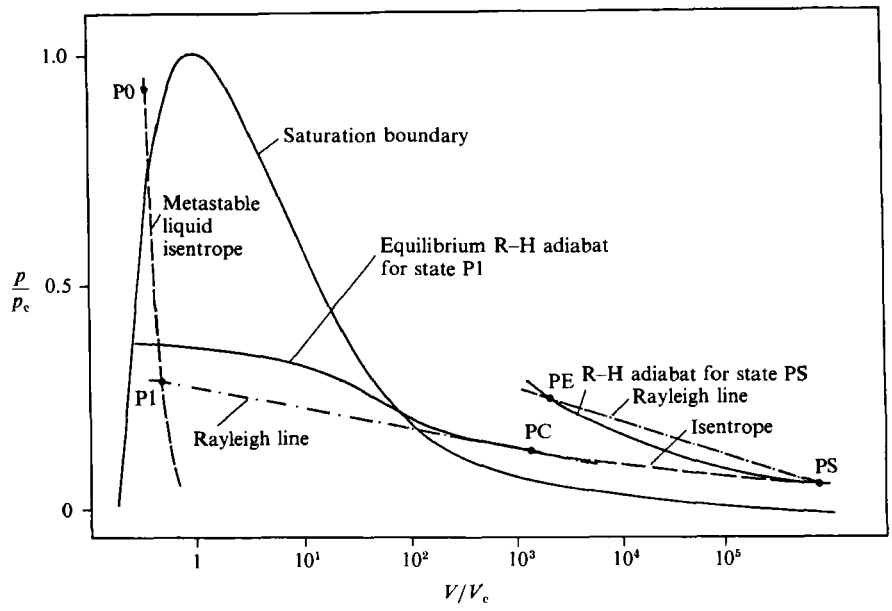

FIGURE 8. Thermodynamical model.

Hugoniot adiabat for state P1, which is in fact always negative, seems to change sign.

As can be seen from the preceding section, state P1 is determined by the interaction of the molecular kinetics of evaporation and the gasdynamic stability criteria for a deflagration discontinuity. This state is therefore not known *a priori*. Unfortunately it is not easy to measure the pressure at the nozzle exit without disturbing the flow within a nozzle of such small dimensions as used here. Such a measurement would determine state P1 and would be an independent check for the developed model. The mass flow rate is insensitive to small changes of the pressure p_1 because p_1 is much smaller than p_0. In order to obtain a pressure value for the state P1, the similarity of supersonic flow (from state PC to state PS in figures 6 and 8) was used: If an axisymmetric supersonic source flow with a source of the diameter of the nozzle and an estimated state P1 is assumed, the pressure behind the closing cylindrical shock has to match the given final pressure p_e at a given distance from the liquid jet core. So the measured distance of the lateral shock is used as an input value for the calculations. The state P1 was found by successive approximations of the calculated final pressure to the experimentally given p_e.

For the calculations a thermal equation of state based on Abbot (1973) and an expression for the specific heat (Thompson & Becker 1979) were used (see the Appendix). Integration of these equations yields expressions for energy, enthalpy, entropy, etc. allowing calculation of all thermodynamic properties. This leads to a closed description of both liquid and gaseous phases of the fluid used, similar to the one given by the van der Waals equation but with somewhat better accuracy. Phase and state changes can then be handled with tools usually used in gasdynamics. Most of the calculations are iterative and no analytical equations can be given. The phase boundary can be reproduced with an accuracy of 3% or better. If a complete phase transition cannot be reached within the evaporation discontinuity, the isentropic two-phase equilibrium sound speed is used as the lower limit for the calculation of the Chapman–Jouguet condition for the state PC.

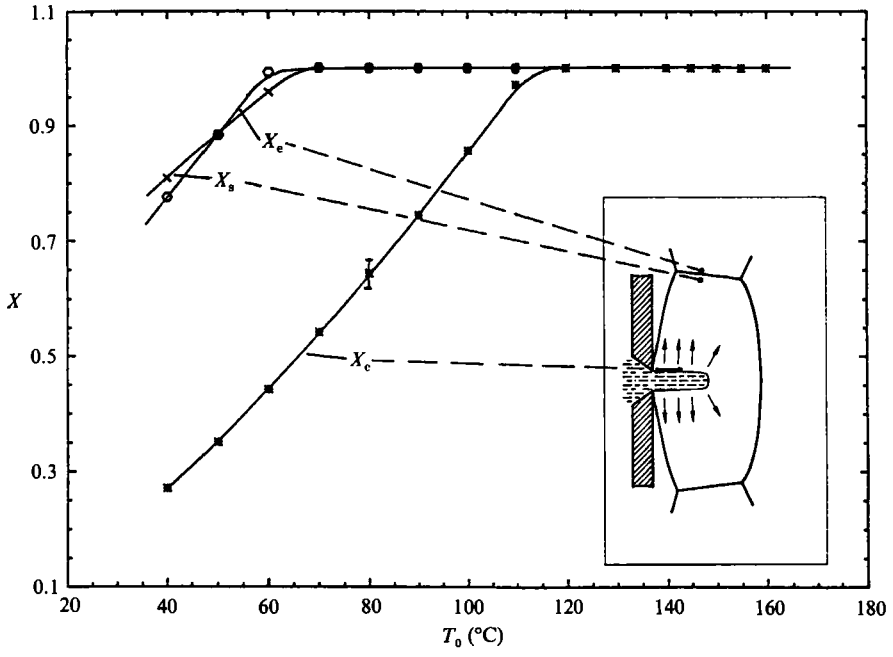

FIGURE 9. Evaporated mass fraction X at the different locations of the model, $p_0 = 15$ bar, $p_e = 10$ mbar. Insert shows a sketch of the jet structure.

5. Results and discussion

A representative result of the calculations is given in figure 9. The mass fraction X of evaporated liquid for the different states PC, PS, and PE (see figures 6 and 8) is plotted as function of the initial temperature ($p_0 = 15$ bar, $p_e = 10$ mbar). $X = 1$ means complete evaporation. As pointed out before, the calculations are only possible for those conditions where experimental values for the distance of the lateral shock are available. Therefore the model can provide results for discrete points only. The lines are plotted for visual guidance. The error bars result from the uncertainty in the determination of the normalized lateral shock distance r/d and indicate the sensitivity of the model calculations to this experimental input value (see also figure 12 and the explanations thereon). The lateral shock distance (r) could be determined on the interferograms with an accuracy of ± 2 nozzle diameters (d). The nozzle diameter itself has deviations of about 10 μm.

By comparing the calculated mass fraction of evaporated liquid X at the different states of the model (PC, PS and PE) with the experimentally determined mass fraction, the validity of the model can be checked. In the experiments the mass fraction was determined by analysing images like those of figures 4 and 10. In particular, complete evaporation can be detected on the shadowgraphs, as they show the opaque liquid parts of the jet only. At $T_0 > 120$ °C the calculations yield complete evaporation for all states downstream of the evaporation discontinuity, which is confirmed experimentally on figures 4(*e*) and 10(*e*).

For lower initial temperatures (e.g. $T_0 = 80$ °C) the evaporation discontinuity is hidden by the departing two-phase flow, but complete evaporation is also reached upstream and downstream of the closing shock structure (figure 10*c*, *d*). At $T_0 = 60$ °C complete evaporation cannot be achieved. The shadowgraph (figure 10*b*) shows a darkened region downstream of the shock structure. The model calculations

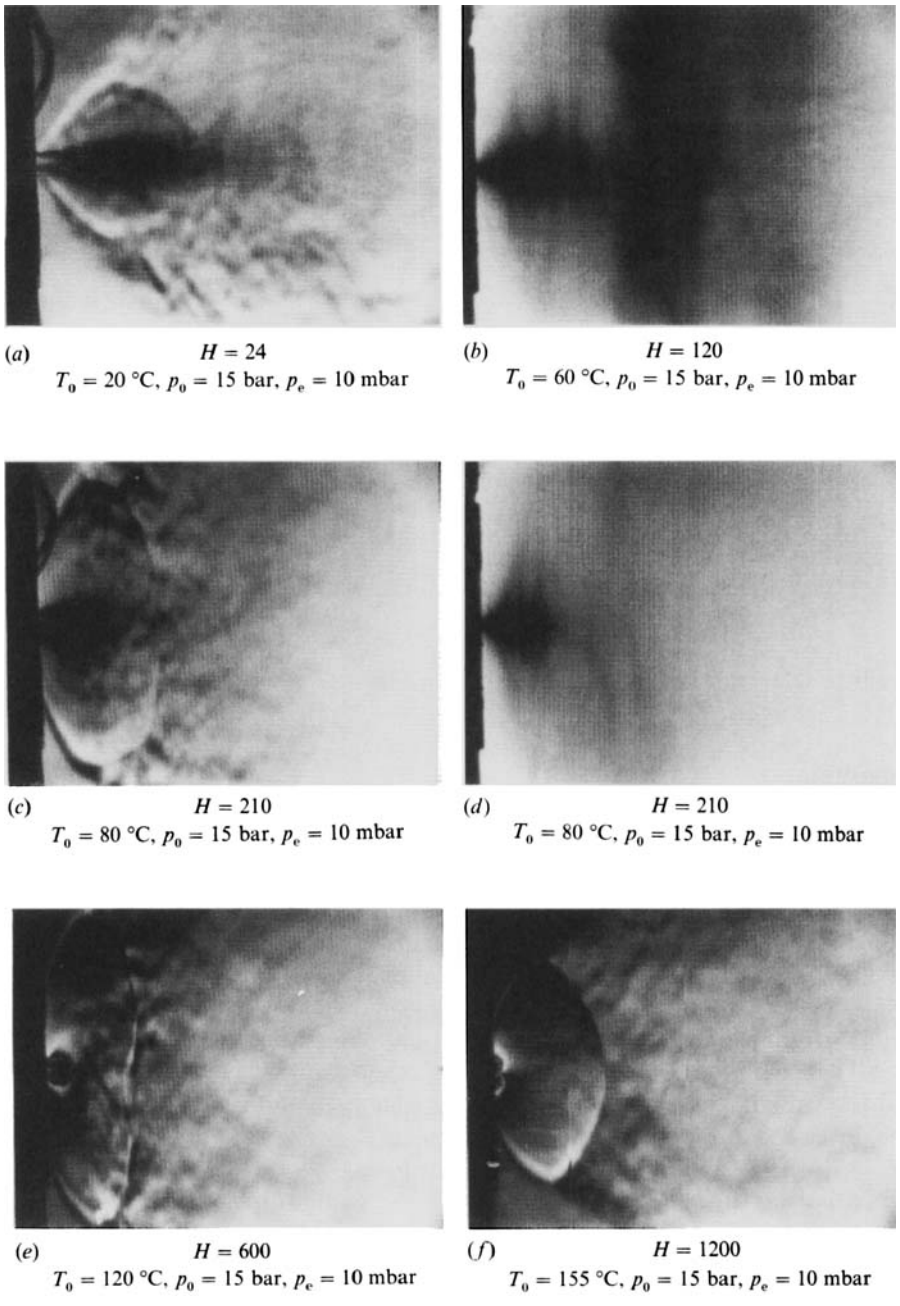

(*a*) $H = 24$
$T_0 = 20$ °C, $p_0 = 15$ bar, $p_e = 10$ mbar

(*b*) $H = 120$
$T_0 = 60$ °C, $p_0 = 15$ bar, $p_e = 10$ mbar

(*c*) $H = 210$
$T_0 = 80$ °C, $p_0 = 15$ bar, $p_e = 10$ mbar

(*d*) $H = 210$
$T_0 = 80$ °C, $p_0 = 15$ bar, $p_e = 10$ mbar

(*e*) $H = 600$
$T_0 = 120$ °C, $p_0 = 15$ bar, $p_e = 10$ mbar

(*f*) $H = 1200$
$T_0 = 155$ °C, $p_0 = 15$ bar, $p_e = 10$ mbar

FIGURE 10. Jets corresponding to calculations of figure 9.

indicate that this is not due to recondensation. In this case the density jump of the fine droplet mist by a factor of 100 within the closing shock is responsible for the light absorption. Real recondensation within the closing shock appears at initial temperatures less than 50 °C as can be seen in figure 9. It should be remembered that condensation within a compression shock wave as well as the complete adiabatic evaporation reported here are effects which can be observed only with substances with retrograde behaviour. Comparable experiments with ethanol ($c_v^* = 10.7$) yield a

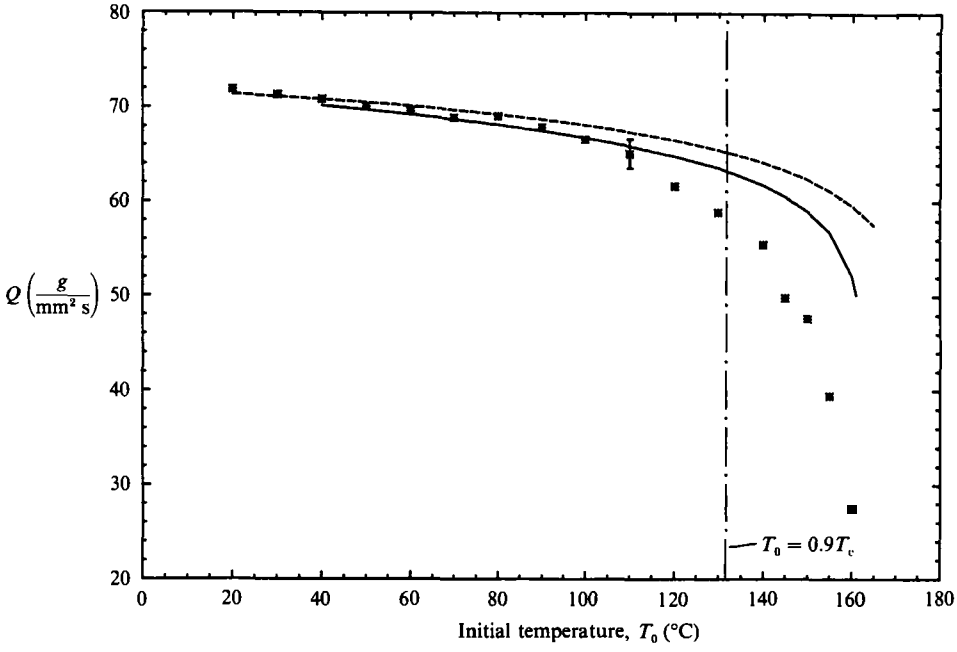

FIGURE 11. Mass flow measurements and model calculations: ----, incompressible calculation; ——, model calculation; *, experimental results. $p_0 = 15$ bar, $p_e = 10$ mbar.

dense opaque droplet cloud darkening the whole visible field. On the other hand, the possibility that in cases with high superheats there might be an evaporation discontinuity and a supersonic region with a shock structure even for non-retrograde substances cannot be excluded. But in fact all this is hidden by the droplet fog.

Figure 10(*a*, *f*) illustrates examples of the limits of applicability of the model. In the first case the initial temperature is too low and the retrograde behaviour not strong enough to permit evaporation on a molecular scale without heat conduction. The liquid is cooled by the evaporating gas and the remaining droplets pass the shock structure on the jet axis owing to their inertia. Therefore the condition of mechanical equilibrium is violated and a homogeneous two-phase flow model is no longer valid. In the second case homogeneous nucleation occurs upstream of the nozzle exit. This leads to a sonic state in the nozzle exit, to choking of the nozzle flow and to a shock structure very similar to that of underexpanded supersonic gas jets (compare with figure 4*f*). This choking occurs when the initial temperature exceeds about 0.9 times the critical temperature T_c and is well known in the literature (Skripov *et al.* 1987).

Figure 11 shows the results of the measurements of the mass flow rate Q corresponding to the experiments of figures 9 and 10. A large deviation of the measured mass flow rate from the model calculations and the incompressible (Bernoulli) estimation is obvious for high initial temperatures. It appears also for temperatures slightly below $0.9T_c$. This is due to the strong, mainly geometrical, simplifications of the model. The real flow field is not only composed of the axisymmetric expansion described by the model, but also of a spherical expansion from the tip of the liquid core of the jet which is not included in the model. This leads first to an underestimation of the measured lateral shock distance, which is an input value of the model calculations, and secondly to something like a weak choking of the nozzle flow. The underestimation of the lateral shock distance could be checked by

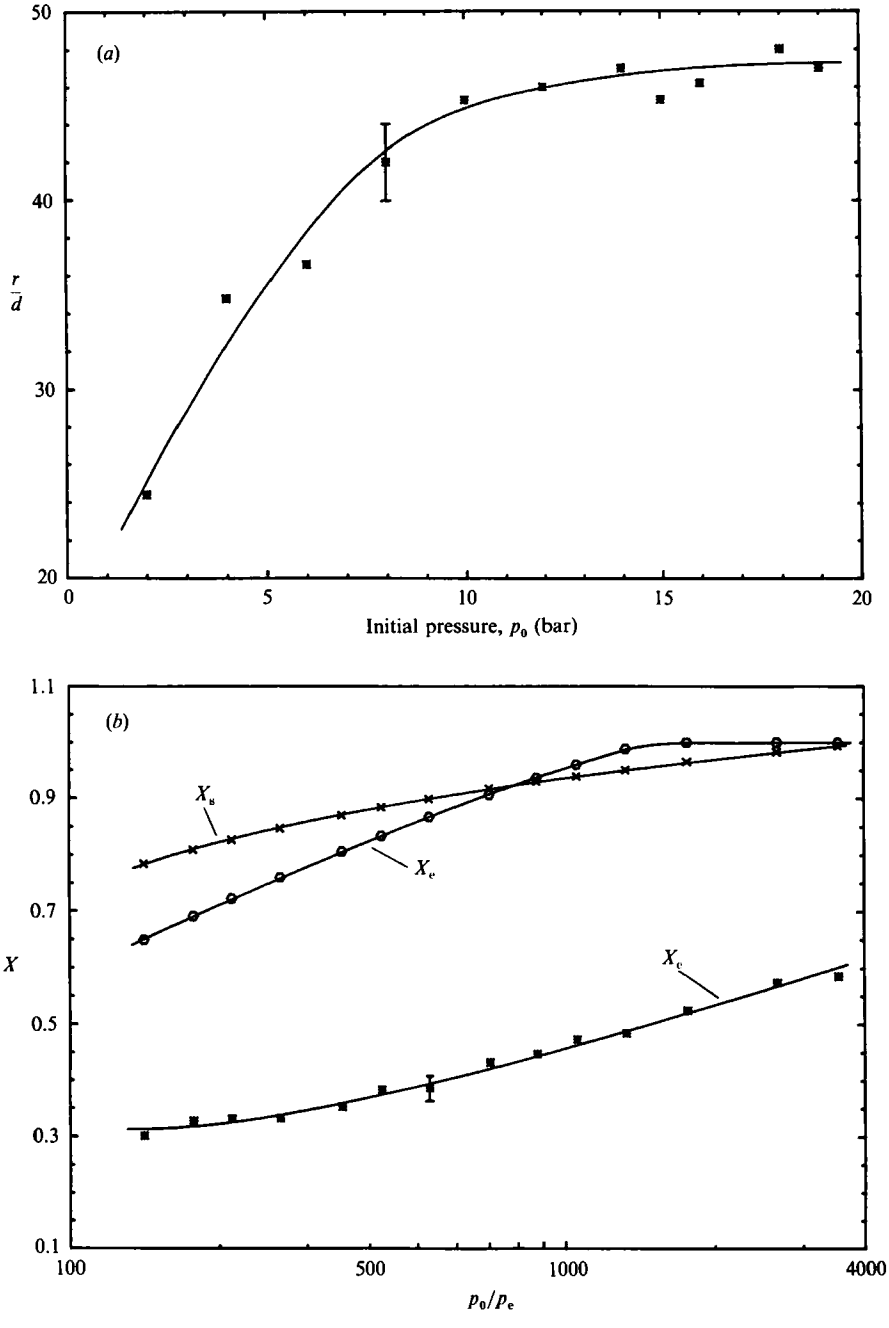

FIGURE 12. (*a*) Lateral shock distance, $T_0 = 20$ °C, $p_e = 2$ mbar. (*b*) Evaporated mass fraction, $T_0 = 57$ °C, $p_0 = 10.6$ bar.

experiments with variable stagnation pressure p_0 and variable final pressure p_e. Within the limits of the model, an increase of p_0 should lead to an increase of the length of the liquid core only, which reduces the influence of the spherical expansion.

Figure 12(*a*) shows, as expected, a limiting value for the distance of the lateral shock. On the other hand all states within the supersonic region of the flow field

should be independent from the final pressure p_e. This could be clearly verified by the optical investigations, which show that the liquid jet core and the two-phase flow departing from it were independent of p_e. In contrast to this the calculations yield an influence on the evaporated mass fraction behind the evaporation discontinuity (X_c in figure 12*b*). They show that an underestimation of the lateral shock distance leads to an overestimation of X_c. For larger values of p_e (small p_0/p_e) the influence of the spherical expansion becomes smaller and the evaporated mass fraction X_c approaches a limiting value again.

6. Concluding remarks

As shown, the experimental results are in good qualitative agreement with the model which has been developed. The quantitative deviations are a consequence of the simplifying assumption of a purely axisymmetric supersonic expansion. The influence of the superposed spherical expansion could be reduced either by a long liquid jet core or by relatively high final pressures. The latter would result in smaller distances of the closing lateral shock. The normalized length of the liquid jet core s/d is limited by homogeneous nucleation of the vapour phase in the bulk of the liquid, which determines the average mean lifetime of the superheated liquid. Larger values of s/d can be reached by increasing the velocity at the nozzle exit (by increasing the stagnation pressure) or by reducing the nucleation volume (by minimizing the nozzle exit diameter).

Within the scope of the model the evaporation rate on the surface of the liquid core is determined by the stability criterion for the deflagration wave and by the demand for sonic outflow from the deflagration. So the nucleation rate, which determines the evaporation rate in the case of the non-diffusion- or non-heat-conducting-limited retrograde phase transition, can be estimated when complete evaporation occurs within this evaporation discontinuity. The interaction of purely gasdynamic mechanisms describing the jet flow with the kinetics of phase transition on a molecular scale by the stability criterion opens this possibility. In this work only a rough estimation could be made because of the influence of the superposed spherical expansion. This leads to a value of about 30 g cm^{-2} s^{-1} for the evaporation rate on the liquid surface ($T_0 = 120$ °C, corresponding vapour pressure = 5.9 bar) when the liquid is expanded to a pressure lower than 0.5 bar. Thompson *et al.* (1987) and Chaves (1984) reported a value an order of magnitude higher. This can be explained by the higher initial temperatures used there ($T_0 > 150$ °C), and by a relaxation wave due to homogeneous nucleation following the so-called forerunner wave in the expansion channel experiments of these authors. Comparable experiments done in this work at the same initial temperatures show homogeneous nucleation within the nozzle with choking and spherical outflow. In this case the model which has been developed is no longer applicable. Labuntsov & Avdeev (1982) also reported a radial outflow and choking of superheated liquid jets with initial temperatures higher than $0.9T_c$. They developed a model with a boiling shock in the nozzle and an upstream state determined by the limit of thermodynamical stability (spinodal condition). In all of the cases reported here, however, the pressure of the superheated liquid state P1 is far above spinodal conditions.

Appendix. Equations of state

The thermal equation of state

$$p_r = \frac{T_r}{Z_c(V_r-1)-(\Omega_c-1)} - \frac{\Omega_c^3+[a_c\Omega_c^2(\Omega_c-1)+\Omega_c^2](T_r-1)}{Z_c^2(V_r-1)^2+\Omega_c Z_c(V_r-1)-\Omega_c^2(\Omega_c-1)} \tag{A 1}$$

is based on Abbot (1973) and was modified by Chaves (1980). The equation is written in reduced form: $p_r := p/p_c$, $V_r := V/V_c$ and $T_r := T/T_c$, where the index c denotes a value at the critical point. It contains three parameters depending on the test substance, C_6F_{14}, used:

$Z_c = p_c V_c/RT_c = 0.267$	the critical compressibility,
$a_c = 8.18$	the Riedel parameter,
$\Omega_c = 0.838$	the critical value of the dimensionless temperature function Ω: $\Omega^3 := \Omega_c^3+[a_c\Omega_c^2(\Omega_c-1)+\Omega_c^2](T_r-1)$.

The expression for the specific heat (Thompson & Becker 1979) is

$$\left.\begin{aligned} c_v &= \frac{Y}{1+Y^2}c_w + c_\alpha \quad \text{for} \quad Y \geqslant 0, \\ c_v &= c_\alpha \qquad\qquad\quad \text{for} \quad Y < 0, \end{aligned}\right\} \tag{A 2}$$

with $Y = \beta(T_r - t)$.

The quotient in (A 2) describes the degree of excitation of the vibrational internal degrees of freedom. c_w (= 54) and c_α (= 3) are the normalized specific heats of the vibrational and the translational/rotational degrees of freedom, respectively, when they are completely excited. β (= 1.08) and t (= 0.389) are parameters determining the temperature dependence of the excitation.

REFERENCES

Abbot, M. M. 1973 Cubic equation of state. *AIChE J.* **19**, 596.

Ashkenas, H. & Sherman, F. S. 1967 The structure and utilization of supersonic free jets in low density wind tunnels. In *4th Intl Symp. on Rarefied Gas Dynamics*, vol. II (ed. J. H. de Leeuw), pp. 84–105. Academic.

Borisov, A. A., Borisov, Al. A., Kutateladze, S. S. & Nakoryakov, V. E. 1983 Rarefaction shock wave near the critical liquid–vapour point. *J. Fluid Mech.* **126**, 59.

Chaves, H. 1980 Verdampfungswellen in retrograden Flüssigkeiten. Diploma thesis, Universität Göttingen; and *Rep.* 24. MPI for Strömungsforschung.

Chaves, H. 1984 Phasenübergänge and Wellen bei der Entspannung von Fluiden hoher spezifischer Wärme. *Mitteilungen aus dem Max-Planck-Institut for Strömungsforschung, Nr.* 77.

Chaves, H., Kurschat, T. & Meier, G. E. A. 1990 Evaporation waves in fluids of high molar specific heat. *Proc. IUTAM Symp. on Adiabatic Waves in Liquid–Vapor systems* (ed. G. E. A. Meier & P. A. Thompson). Springer.

Chaves, H., Lang, H., Meier, G. E. A. & Speckmann, H.-D. 1985 Adiabatic phase transitions and wavesplitting in fluids of high specific heat. In *Lecture Notes in Physics*, vol. 235, p. 115. Springer.

Dettleff, G., Meier, G. E. A., Speckmann, H. D., Thompson, P. A. & Yoon, C. 1982 Experiments on shock liquefaction. In *Proc. 13th Intl Symp. on Shock Tubes and Waves* (ed. C. E. Trainorand & J. G. Hall). State University of New York Press.

DETTLEFF, G., THOMPSON, P. A., MEIER, G. E. A. & SPECKMANN, H.-D. 1979 An experimental study of liquefaction shock waves. *J. Fluid Mech.* **95**, 279.

FUCHS, H. & LEGGE, H. 1979 Flow of a water jet into vacuum. *Acta Astronautica* **6**, 1213.

KURSCHAT, TH., CHAVES, H. & MEIER, G. E. A. 1991 A simple analytical model for the evaluation of the free-jet Mach-disk location. *Phys. Fluids* (submitted).

LABUNTSOV, D. A. & AVDEEV, A. A. 1982 Mechanism of flow blockage involving shock boiling of liquid. *High Temp.* **20**, 81.

LAMBRAKIS, K. C. & THOMPSON, P. A. 1972 Existence of real fluids with negative fundamental derivative. *Phys. Fluids* **15**, 933.

LANDAU, L. D. & LIFSCHITZ, E. M. 1966 *Lehrbuch der Theoretischen Physik*, vol. IV, Kap IX and XIV. Akademic-Verlag.

LIENHARD, J. H. & DAY, J. B. 1970 The breakup of superheated liquid jets. *Trans. ASME* D: *J. Basic Engng* **92**, 515.

SIDORENKO, A. D. 1968 Wave adiabates for media with arbitrary equation of state. *Sov. Phys. Dokl.* **13**, 117.

SIDORENKO, A. D. 1982 Wave adiabatic curves for media with arbitrary state equation. *Appl. Math. Mech.* **46**, 241.

SKRIPOV, V. P. 1974 *Metastable Liquids*. Wiley.

SKRIPOV, V. P., BAYDAKOV, V. G. & MAL'TSEV, S. A. 1987 'Vapour explosion' in liquid argon or methane discharged through short ducts. *heat Transfer Sov. Res.* **19**, 133.

THOMPSON, P. A. & BECKER, F. 1979 A one-parameter thermal-caloric corresponding-states model. *Chem. Engng Sci.* **34**, 93.

THOMPSON, P. A., CAROFANO, G. C. & KIM, Y.-G. 1986 Shock waves and phase changes in a large-heat-capacity fluid emerging from a tube. *J. Fluid Mech.* **166**, 57.

THOMPSON, P. A., CHAVES, H., MEIER, G. E. A., KIM, Y.-G. & SPECKMANN, H.-D. 1987 Wave splitting in a fluid of large heat capacity. *J. Fluid Mech.* **185**, 385.

THOMPSON, P. A. & LAMBRAKIS, K. C. 1973 Negative shock waves. *J. Fluid Mech.* **60**, 187.

THOMPSON, P. A. & SULLIVAN, D. A. 1975 On the possibility of complete condensation shock waves in retrograde fluids. *J. Fluid Mech.* **70**, 639.